ELSEVIER

International Journal of Heat and Fluid Flow 21 (2000) 420–431

International Journal of HEAT AND FLUID FLOW

www.elsevier.com/locate/ijhff

Numerical analysis of depressurisation of highly pressurised liquid propane

M.A. Aamir, A.P. Watkins *

Mechanical Engineering Department, UMIST, Manchester M60 1QD, UK

Received 19 January 1999; accepted 13 December 1999

Abstract

This investigation consists of two parts: one upstream of the breach and the other downstream. The first part involves construction of a thermodynamic model of the fluid flow, based on a quasi-steady-state separated flow analysis. The model includes qualitative as well as quantitative description of the exit conditions together with an initial drop size distribution required to define the flow field at the exit of the breach. These flow field parameters are used as the inlet conditions to the spray model, which is used downstream of the breach. The discrete droplet model in a two-dimensional, axi-symmetric, cylindrical-polar co-ordinate system is used. Modified droplet collision and break-up models are introduced to model the dense aspects of the spray. The results predicted by the theoretical spray model at 95, 500 and 1028 mm from the nozzle, have been successfully validated against the experimental data obtained from two independent sources.

Keywords: Spray modelling; Propane blowdown; CFD analysis

1. Introduction

Pressure vessels are widely used to store liquefied gases under pressure at ambient temperature. Many accidents in chemical plants and offshore oil and gas platforms result in the spillage of these toxic, radioactive, flammable or explosive materials, from such pressure vessels. In the past few years, interest in the hazard associated with a loss of containment of such liquefied gases has become relatively more important (Chen et al., 1995). A typical accident scenario involves a pressurised vessel, filled with liquid propane, and fitted with a draw-off pipe. Lees (1980) found that in such a case, the probability of a leak appearing in the piping is more than that in the pressure vessel. If a breach occurs, liquid moving isothermally from a high pressure zone to a low pressure zone often crosses the bubble point curve and disintegrates into a spray by partial evolution of vapour. Accurate prediction of the spray discharged is important in determining the consequences of the accident.

In late 1980s, simultaneous independent work started in France (Hervieu, 1991) and in UK (Bettis and Jaggers, 1992). The working liquid in both the laboratories was propane (Hervieu, 1992). The experimental set-up consisted of a storage vessel, a draw-off pipe and a nozzle representing the breach. The experimental work at the Health and Safety Executive laboratory (HSE) (Allen, 1996a,b) managed to give an in-depth analysis of the state of the spray in terms of droplet size distributions and velocity profiles both in the axial and radial directions and at the centre line. But reliable data were obtained only at a distance of 500 and 1028 mm from the nozzle. Hervieu and Veneau (1996) reported experimental axial velocity and droplet size at the centreline, 95 mm from the nozzle, but did not capture the spray itself. An outline diagram of their experimental set-up is shown in Fig. 1. A similar setup was used by Allen (1996a,b). The difference was that Hervieu and Veneau (1996) employed Phase Doppler Particle Analyser (PDPA) to measure the liquid droplet size and velocity; while Allen (1996a) used Laser Doppler Anemometry (LDA) system for velocity measurements and Malvern particle sizer for propane droplet size distribution measurements. The liquid propane was saturated in both conditions stored at room temperature.

Pereira and Chen (1996) and Vandroux-Koenig and Berthoud (1997) tried to model the spray but their calculated results were far from the experimental results (Hervieu and Veneau, 1996). Pereira and Chen (1996) used the Eulerian Lagrangian approach, treating the air–vapour mixture phase with Eulerian formulation while droplet phase was handled using the Lagrangian formulation. They used a thin-skin evaporation model and a modified k–ε model to account for anisotropy of turbulence but ignored the effects of droplet collisions and break-up. They did not compare their results with any experimental data, but Vandroux-Koenig and Berthoud (1997) found Pereira-Chen's (1996) numerical predictions to be far from the experimental results (Hervieu and

* Corresponding author.

E-mail addresses: muhammad.aamir@stud.umist.ac.uk (M.A. Aamir), paul.watkins@umist.ac.uk (A.P. Watkins).

0142-727X/00/$ - see front matter
PII: S0142-727X(00)00002-3

Notation

A	cross-sectional area
B_H	heat transfer number
C_d	drag force coefficient
C_D	discharge coefficient
C_P	specific heat at constant pressure
D	drop diameter
D_{AB}	binary diffusion coefficient
f	vapour mass fraction, random number
H	specific enthalpy
I	turbulence intensity
i, j	grid parameters
K_d	droplet momentum coefficient
k	turbulence kinetic energy
l_t	turbulence length scale
m	mass
$\dot{m}$	mass flow rate
N	number of drops in a parcel
n	Rosin–Rammler distribution coefficient
p	pressure
R_c	critical pressure ratio
Re	Reynolds number
r	radial co-ordinate
r_{inj}	injection radius
T	temperature
t	time
Δt	time interval
U, V	axial and radial velocities
V	volume
u', v'	fluctuating components of respective velocities
We	Weber number
XX, YY	random numbers
x	mass fraction, axial co-ordinate
x_0	length of the injection cell

Greeks

α	void fraction
β	half spray cone angle
ε	rate of dissipation of turbulence kinetic energy
γ	ratio of specific heats
ν	collision frequency
ρ	density
σ	surface tension

Subscripts

a	air
atm	atmospheric conditions
b	bag break-up
c	critical, discharge coefficient
d	drop
f	liquid propane
g	gas and vapour mixture
inj	injection
n	nozzle
P	pipe
pv	pressure vessel
r	ratio
rel	relative
rem	removed
s	strip break-up
T	total
v	propane vapour
wb	wet bulb

Superscripts

n	new
o	old

Veneau, 1996). Vandroux-Koenig and Berthoud (1997) used an Eulerian–Eulerian approach where both the phases are modelled using Eulerian transport equations, with the Prandtl mixing length model to evaluate turbulent viscosity terms. Thus they did not take particle diffusivity into account, and the modelling resulted in propane droplets remaining in the centre of the jet. This gave low evaporation rates, which meant that the calculated results were far away from the experimental ones.

The present authors also made an earlier attempt at modelling the propane spray (Aamir and Watkins, 1998), but the model used was assumed to have no droplet break-up and collisions. So far, there has not been any other successful attempt reported in the literature to model the propane spray, with given reported experimental conditions. Here we have attempted to model the liquid flow from the pressure vessel to the nozzle and to model the dense spray evolving from the nozzle.

In the first part of this paper, a thermodynamic model is described which identifies the flow from the pressure vessel to the nozzle via a pipe. Due to the low-pressure region available in the pipe, propane tends to flash evaporate. It has been theorised that after the initial nucleation of the bubbles, the vapour will be more likely to form at the bubble surface, causing rapid growth of the bubble and a corresponding physical displacement of the adjacent liquid. On passing through the nozzle, the displacement will cause the disintegration of the liquid, resulting into formation of a spray. This is unlike the work of Vandroux-Koenig and Berthoud (1997), who assumed the flash evaporation to take place downstream of the nozzle; here a methodology similar to a discharge from a pressurised metered dose inhaler (pMDI) developed by Dunbar and Watkins (1997) is followed. Their model considered separated flow methodology while neglecting the metastability of the fluid in the expansion chamber. They found that the primary atomisation process was dominated by flash evaporation of the superheated liquid within the nozzle. This was modelled by assuming that the liquid would instantaneously flash evaporate upon entering the nozzle, the percentage liquid that could flash evaporate being calculated using a simple adiabatic heat balance calculation. They applied Bernoulli's equation to obtain mass flow rates for the sub-critical discharge and assumed then ideal gas equation to be valid for critical discharge. The authors of this paper have followed a similar methodology.

Apart from Dunbar's model there have been many studies pertaining to two-phase flow inside the nozzle. Fauske (1965) reported data on critical air–water flows in tubes and channels at low pressures for a large range of qualities and gave a nonequilibrium slip model to predict the data. He found that the phenomena controlling the critical flow in one-component mixtures are the same as for two component mixtures. Graziadio et al. (1987) tested internal mixing twin fluid atomiser with different coal–water fuels. They interpreted their measurements by semi-empirical correlations based on mechanistic models of the flow within the atomiser and found that the flow structure within the model is not influenced by the physical properties of the fuel. He and Ruiz (1995) studied the effect of cavitation on flow and turbulence in plain orifices for high-speed atomisation. They formulated the process equations to

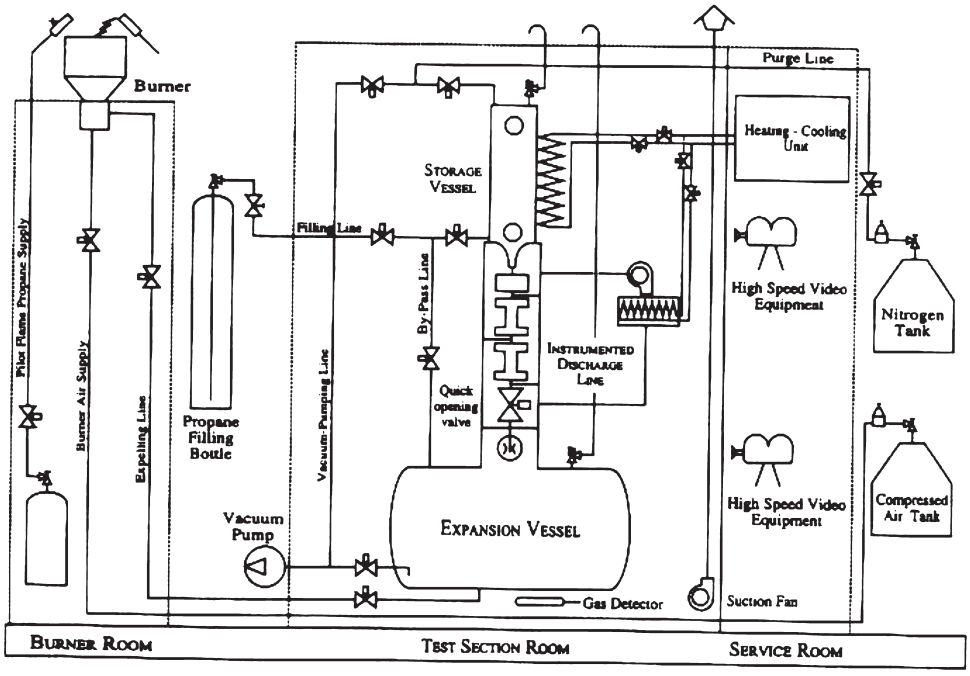

Fig. 1. The experimental setup (*Source*: Hervieu and Veneau, 1996).

calculate the discharge coefficient and the conditions on the onset of cavitation from first principles. Their model thus explained the reason for sudden increase in spray angle observed in diesel fuel injectors at the onset of cavitation, based on the reason that the turbulence in the cavitating flow is higher and decays more slowly than that in the noncavitating flow. Similarly Schmidt et al. (1999) constructed a numerical model that treated liquid and vapour as continua for predicting small-scale, high-speed, cavitating nozzle flow. This model successfully predicted coefficient of discharge and exit velocity for a variety of nozzle geometries.

None of the above works, apart from Dunbar and Watkins (1997), involved the flashing nature of the problem described here. The only problem remains whether the usage of sonic discharge of an ideal gas under adiabatic conditions, be applicable. Graziadio et al. (1987) showed that their experimental measurements of air mass velocity in the exit holes followed ideal gas laws when fuel mass velocity is equal to zero. It can be shown from their work that for a high pressure upstream of the nozzle, and low fuel mass flux, there is an acceptable error in over-predicting the experimental data. With the main aim of this project being the definition of spray and not the flow upstream of the nozzle, Dunbar's model, which accounted for flashing phenomena, was used. It will be shown later that the results downstream of the nozzle follow the experimental results within acceptable error limits, thus qualitatively validating the assumption made upstream of the nozzle.

In the second part of this paper, the mathematical modelling, based on Eulerian–Lagrangian approach, of the multiphase propane jet is presented. The model is similar to the Discrete Droplet Model (DDM) described by Faeth (1983). Droplet break-up models and a modified collision model are included to account for the dense spray involved. These are described later. Results are presented in the third part.

There has been a significant effort in the literature to understand the events that occur when two or more drops collide (Orme, 1997). The majority of the early work was focussed on the droplet growth relating to precipitation and was thus limited to water droplet collision phenomena. Later studies have sought information on the collision behaviour of fuel droplets for applications to combustion spray systems. Researchers (Orme, 1997) have found distinct differences between the collision behaviour of water droplets and fuel droplets. For phenomenological reasons, the behaviour of droplet collisions is found to be dependant on the surface tension and viscosity of the droplet fluid as well as the gas density, pressure and viscosity. Since there has been no experimental study of high-pressure liquid propane drops, it was assumed to act similar to diesel fuel. Therefore break-up and collision models used in engine spray codes have been used in this code developed in-house as well. Details of the models and their modifications are presented later in the paper.

2. Modeling for flow field at nozzle exit

It is intended to use the discrete droplet model (DDM) to simulate the spray emerging from a pressure vessel via a nozzle. Like other separated flow (SF) models described by Faeth (1983), the DDM needs input of the flow field at the nozzle exit. Due to lack of any quantitative experimental data at the exit of the nozzle, the development of a model to define the flow field in this region is imperative. A theoretical model of two phase flow from a pressure vessel into a pipe fitted with a nozzle to atmosphere is described here. It is similar to the description of actuator flow in a pMDI modelled by Dunbar and Watkins (1997).

The mass of propane in the pressure vessel at the new time step is calculated as follows:

$$m_{\mathrm{pv}}^{\mathrm{n}} = m_{\mathrm{pv}}^{\mathrm{o}} - \dot{m}_{\mathrm{pv}}\Delta t, \tag{1}$$

where

$$\dot{m}_{\mathrm{pv}} = A_{\mathrm{P}} C_{\mathrm{D_P}} \left[2\rho_{\mathrm{f}}\left(p_{\mathrm{pv}} - p_{\mathrm{P}}\right)\right]^{0.5}. \tag{2}$$

The total enthalpy in the pressure vessel can be calculated at a new time level by means of an energy balance.

$$(m_f h_f + m_v h_v)^n_{pv} = H^o_{pv} - \dot{m}_{pv}\overline{h}^o_{pv}\Delta t - \left(m^n_v - m^o_v\right)_{pv} h^n_{fv}, \quad (3)$$

where $\overline{h}^o_{pv}$ is the mass average enthalpy at the previous time step.

Assuming that the propane vapour generated in the pressure vessel remains in the pressure vessel, and that $\dot{m}_{pv}$ is all liquid, the mass of liquid in the pipe at the new time step is given as

$$(m^n_f)_P = (m^o_f)_P + \dot{m}_{pv}\Delta t - \dot{m}_P\Delta t. \quad (4)$$

At time $t = 0$, there must be air in the pipe. Hence a quasi-steady state energy balance for a small time step Δt gives

$$H^n_P = H^o_P + (\dot{m}h)_{pv}\Delta t - (\dot{m}h)_P\Delta t, \quad (5)$$

where

$$H^n_P = [(m_f + m_v)h_f + m_v h_{fv} + m_a h_a]^n_P. \quad (6)$$

Mainly, flow evaporation is assumed to occur when the fluid enters the nozzle. In order to calculate the mass flow rate through the nozzle, the fractional mass of liquid entering the nozzle that could flash-off, must be calculated. This is done by performing a simple adiabatic heat balance to obtain the quantity of liquid that could flash within the pipe, as follows:

$$x_{flash} = \frac{h_f(T_P) - h_f(T_{wb})}{h_{fv}(T_{wb})}. \quad (7)$$

The wet bulb temperature is taken as the temperature of saturated propane at atmospheric pressure and is assumed constant throughout the calculations for the spray: as the temperature of the liquid propane.

The critical pressure ratio through the nozzle is given as

$$R_c = \left(\frac{2}{\gamma + 1}\right)^{\gamma/\gamma - 1}. \quad (8)$$

Flow is sub-critical if

$$R_c < \frac{p_{atm}}{p_P} \quad (9)$$

and super-critical if

$$R_c > \frac{p_{atm}}{p_P}. \quad (10)$$

For a sub-critical flow, velocities of the individual phases are calculated from Bernoulli's equation as follows:

$$U_{f,g} = \left(\frac{2(p_P - p_{atm})}{\rho_{f,g}}\right)^{0.5} \quad (11)$$

and mass flow rates are given as

$$\begin{aligned} \dot{m}_f &= A_c(1 - x_P)\rho_n U_f, \\ \dot{m}_g &= A_c x_P \rho_n U_g, \\ \dot{m}_T &= \dot{m}_f + \dot{m}_g, \end{aligned} \quad (12)$$

where A_c = product of cross-sectional area of the nozzle and discharge coefficient and

$$\rho_n = \frac{\rho_f \rho_g}{x_P \rho_f + (1 - x_P)\rho_g}. \quad (13)$$

A constant value of discharge coefficient of 0.73 is assumed. For critical flow

$$U_{g,c} = \left(\frac{\gamma p_P R_c^{\gamma - 1/\gamma}}{\rho_g}\right)^{0.5}, \quad (14)$$

$$U_{f,c} = \left(\frac{2(p_P - p_P R_c)}{\rho_f}\right)^{0.5}. \quad (15)$$

After applying this thermodynamic model, quality, density, velocity, energy and void fraction are obtained at the nozzle exit, which are then used as input to the spray code. Due to the lack of any correlation to describe the atomisation phenomenon of flashing type, different empirical correlations of other types of atomisers were used to model the atomisation process and evaluate the drop diameter. But none could predict the sort of drop diameters required to model the experimental results at 95 mm from the nozzle. Therefore, a Rosin–Rammler (R–R) distribution was used to define the droplet size distribution at the nozzle exit. A typical volumetric R–R distribution is given as

$$f(D_d) = \frac{0.693 n D_d^{n-1}}{D_{32}^n} \exp\left(-\frac{0.693 D_d^{n-1}}{D_{32}^n}\right). \quad (16)$$

The values of n and D_{32} were optimised by validating the calculated results using the experimental data at the centreline, 95 mm from the nozzle, as is explained later in this paper.

3. Modeling of propane spray

The DDM describes the continuous gas phase and dispersed liquid phase as separate media, which communicate via source terms, to capture momentum exchange and heat and mass transfer between each phase. The huge number of drops experienced in real sprays is represented by discrete droplet parcels which account for groups of drops which are assumed to be identical in terms of size, position, velocity, time, temperature and density. Thus, only a small number of droplet parcel calculations are required to represent the transport of the drops contained within the spray, similar to a Monte Carlo procedure. The transport equations for the discrete liquid phase are formulated as Lagrangian conservation equations and describe the transport of each individual droplet parcel. The structure of heat and mass transfer equations take the form proposed by Dunbar and Watkins (1997), where the governing equations are modified to include convection effects. The droplet trajectory can be obtained by integrating the following equations:

$$\frac{dx_d}{dt} = U_d, \quad (17)$$

$$\frac{dr_d}{dt} = V_d. \quad (18)$$

The general equation for particle motion, known as the Bassett, Boussinesq and Oseen (BBO) equation, has been simplified assuming negligible role of virtual mass and Bassett forces at atmospheric conditions, while also ignoring the Saffman force and Magnus effect. Thus a simplified general equation of particle motion that only describes the inertial and drag forces acting on the sphere can be derived and the droplet momentum equations can be written in the following form:

$$\begin{aligned} \frac{dU_d}{dt} &= K_d\left(U + u' - U_d\right) - \frac{1}{\rho_d}\frac{\partial p}{\partial x}, \\ \frac{dV_d}{dt} &= K_d\left(V + v' - V_d\right) - \frac{1}{\rho_d}\frac{\partial p}{\partial r}, \end{aligned} \quad (19)$$

where K_d is the droplet momentum coefficient given by

$$K_d = \frac{3}{4} C_d \frac{\rho}{\rho_d}\frac{1}{D_d} U_{rel}. \quad (20)$$

The relative velocity between the liquid and gas phase, U_{rel} is defined as

$$U_{\rm rel} = \left(\left(U + u' - U_{\rm d} \right)^2 + \left(V + v' - V_{\rm d} \right)^2 \right)^{0.5} \tag{21}$$

and $C_{\rm d}$ is given as

$$C_{\rm d} = \begin{cases} 0.44 & \text{for } Re > 1000, \\ \frac{24}{Re}(1 + 0.15Re^{0.687}) & \text{for } Re \leqslant 1000. \end{cases} \tag{22}$$

Dunbar and Watkins (1997) proposed that the droplets in case of flash evaporation can be assumed to be at wet-bulb temperature. At this temperature the heat and mass transfer numbers become equal. Hence they modified Faeth's (1983) model to the following form:

$$\dot{m}_{\rm d} = -\pi D_{\rm d} \rho_{\rm g} D_{AB} Sh \ln(1 + B_{\rm H}), \tag{23}$$

where Sh is the Sherwood number defined as

$$Sh = 2 + \frac{0.556\ Re^{0.5} Sc^{1/3}}{\left(1 + \frac{1.232}{Re\ Sc^{4/3}}\right)^{0.5}}. \tag{24}$$

Sc is the Schmidt number and $B_{\rm H}$ is the heat transfer number given as

$$B_{\rm H} = \frac{C_{\rm P,g}\left(T_{\rm g} - T_{\rm d}\right)}{h_{\rm fg}}. \tag{25}$$

Here $C_{\rm P,g}$ is the mass weighted specific heat of vapour–air mixture.

The turbulent dispersion of the drops is simulated using the eddy interaction model of Gosman and Ioannides (1981). In this model, the droplet parcels are assumed to interact with individual eddies, whose properties are approximated stochastically from the turbulence properties of the gas phase, resulting in the deflection of the droplet parcel trajectory whilst residing within the turbulent eddy. The gas phase turbulence transport is represented by the high Reynolds number k–ε model of Launder and Spalding (1972), which assumes isotropy of turbulence. The k–ε model, although it solves this problem in a 2D axi-symmetric form, does account for the dispersion of the drops in the third direction, due to its isotropic nature.

3.1. Break-up and collision models

The drop break-up is modelled following the correlations given by Nicholls (1972) for two different break up regimes. Droplets are assumed to become unstable and undergo break up similar to a bag break up mechanism when

$$We = \frac{\rho_{\rm g} V_{\rm rel}^2 D}{2\sigma} > 6.0, \tag{26}$$

where

$$V_{\rm rel} = \left(\left(\overline{U} - U_{\rm d} \right)^2 + \left(\overline{V} - V_{\rm d} \right)^2 \right)^{0.5}. \tag{27}$$

$\overline{U}$ and $\overline{V}$ are the average gas velocity in the Eulerian gas phase cell, in which the drop resides. Following Reitz and Diwakar (1986), the corresponding life of the unstable drop for the bag break up is assumed to be proportional to the drop natural frequency given as

$$t_{\rm b} = \pi \left(\frac{\rho_{\rm d} D^3}{16\sigma} \right)^{0.5}. \tag{28}$$

In stripping mode, the drop break up criterion is given as

$$\frac{We}{\sqrt{Re}} > 0.5, \tag{29}$$

and the corresponding life time of the unstable drop for stripping break-up is given by

$$t_{\rm s} = C_{\rm s} \frac{D}{2V_{\rm rel}} \sqrt{\frac{\rho_{\rm d}}{\rho_{\rm g}}}. \tag{30}$$

A modified version of the statistical approach used by O'Rourke and Bracco (1980) for droplet collision and coalescence has been used in this study. In this approach, it is assumed that the droplets of the same parcel do not collide, as they are all moving with the same velocity, and collision occurs only between those parcels which are in the same computational cell. The number of droplet parcels remain the same in the overall computational domain, unless all the droplets in the smaller sized parcel are absorbed by the collector parcel, in which case the number of parcels is reduced by one.

The collision frequency of a collector drop with all the droplets in the other parcel is given by

$$v = \frac{N_2}{V_{\rm cell}} \frac{\pi}{4} (D_1 + D_2)^2 \left| U_{\rm d,1} - U_{\rm d,2} \right|, \tag{31}$$

where $V_{\rm cell}$ is the cell volume, subscripts 1 and 2 refer to the parcel with larger diameter drops(collector) and parcel with smaller diameter drops, respectively and N is the number of drops in the respective parcel. The probability that a collector drop undergoes n collisions with the other droplets during a time step is given by Poisson distribution as

$$P_{\rm n} = {\rm e}^{-\overline{n}} \frac{\overline{n}^n}{n!}, \tag{32}$$

where $\overline{n} = v\Delta t$ and the probability of no collision is $P_0 = {\rm e}^{-\overline{n}}$. A random number XX is chosen within the interval (0,1) and if $XX < P_0$, no collision occurs. Otherwise collision occurs and it can be either coalescence of drops or grazing collision. Another random number YY is chosen and compared with a probability parameter for coalescence $E_{\rm coal}$ given by O'Rourke and Bracco (1980), as

$$E_{\rm coal} = {\rm Min}\left[\frac{2.4}{We_{\rm d,2}} \left(D_{\rm r}^3 - 2.4 D_{\rm r}^2 + 2.7 D_{\rm r} \right), 1.0 \right], \tag{33}$$

where $D_{\rm r} = D_2/D_1$.

If $YY \leqslant E_{\rm coal}$ then the collision results in coalescence, otherwise grazing collision is assumed. In the literature the number of droplets (nr) which collide with each collector drop is obtained from

$$\sum_{k=0}^{nr-1} P_k \leqslant XX \leqslant \sum_{k=0}^{nr} P_k, \tag{34}$$

where the P_k's are obtained from the Poisson distribution. However, in the work reported here, a time step limitation associated with the drop coalescence is also taken into account, which states that the computational time step Δt be small compared to the collision time $\Delta t_{\rm d}$ for the droplets. If this condition is fulfilled then the probable number of droplets that coalesce in a time step will be $n_{\rm rem} = v_{\rm d} \Delta t N_2$, where $v_{\rm d}$ is given as

$$v_{\rm d} = \frac{1}{\Delta t_{\rm d}} = \frac{N_1}{V_{\rm cell}} \frac{\pi}{4} (D_1 + D_2)^2 \left| U_{\rm d,1} - U_{\rm d,2} \right|. \tag{35}$$

Hence the minimum of nr and $n_{\rm rem}/N_1$ is taken, and accordingly the velocity and the drop diameters of the collector parcel are adjusted as suggested by O'Rourke and Bracco (1980).

When a grazing collision occurs, no mass is exchanged between the droplet parcels, but there may be exchanges of momentum and energy. These exchanges are also adjusted as suggested by O'Rourke and Bracco (1980).

3.2. Gas phase

The solution domain for the general gas phase transport equation is defined in cylindrical-polar co-ordinates for a two-dimensional axi-symmetric framework, yielding the following:

$$\frac{\partial}{\partial t}(\rho\alpha\phi)+\frac{\partial}{\partial x}(\rho\alpha U\phi)+\frac{1}{r}\frac{\partial}{\partial r}(r\rho\alpha V\phi) = \frac{\partial}{\partial x}\left(\Gamma_\phi\alpha\frac{\partial\phi}{\partial x}\right)+\frac{1}{r}\frac{\partial}{\partial r}\left(r\Gamma_\phi\alpha\frac{\partial\phi}{\partial r}\right)+\alpha S_\phi+S_\phi^{\mathrm{d}}. \tag{36}$$

The general variable ϕ represents the following: 1 (for mass conservation), U, V, f, h, k and ε. Additional terms have been introduced into the general gas phase transport equation to accommodate the interactions with the dispersed liquid phase. These are the void fraction, which is defined as the volume fraction of gas

$$\alpha=\frac{V_{\mathrm{g}}}{V_{\mathrm{g}}+V_{\mathrm{d}}}, \tag{37}$$

and the liquid phase source term, S_ϕ^{d}, which communicate the interactions of momentum and heat and mass transfer from the dispersed liquid phase to the gas phase. The turbulence transport is represented by the high Reynolds number k–ε model of Launder and Spalding (1972), while the gas phase source terms, S_ϕ, the diffusion coefficients, Γ_ϕ and the liquid source terms can also be found in the literature (Khaleghi, 1990). Air–vapour mixture properties are taken where ever required.

3.3. Numerical procedure

The solution domain is defined in a two-dimensional, axi-symmetric, cylindrical–polar co-ordinate system. A finite volume staggered grid approach is used to solve the Eulerian gas phase transport equations. The hybrid scheme is used for spatial discretisation, while the Euler implicit scheme is employed for temporal discretisation. The PISO scheme developed by Issa (1986) is introduced to handle the coupling between the pressure and the velocity. Gas and droplet velocity equations are solved simultaneously. The liquid phase source terms in the gas phase momentum equations introduce the new time level velocities for both the gas and liquid phases simultaneously due to the implicit approximation of the temporal discretisation. The gas phase momentum equations are therefore solved by substituting the discretized droplet momentum equations into the gas phase momentum equations, resulting in modified source terms. Khaleghi (1990) gives the mathematical details of this process.

It is relatively simple to discretize the liquid phase transport equations because of their Lagrangian formulation. The Euler implicit temporal differencing scheme is employed to discretize the droplet trajectory, momentum and evaporation equations over the same time step used in the discretisation of the gas phase equations. The discrete droplet evaporation equations are solved by following the procedure developed by Wang (1992) as follows:

$$m_{\mathrm{d}}^{\mathrm{n}}=m_{\mathrm{d}}^{\mathrm{o}}-\pi D_{\mathrm{d}}\rho_{\mathrm{g}}^{\mathrm{n}}D_{AB}Sh^*\Delta t, \tag{38}$$

where

$$Sh^*=Sh\,\ln(1+B_{\mathrm{H}}). \tag{39}$$

The new time level droplet mass is given as:

$$m_{\mathrm{d}}^{n}=\frac{\pi\left(\rho_{\mathrm{d}}D_{\mathrm{d}}^3\right)^{\mathrm{n}}}{6}. \tag{40}$$

Solving the above equations simultaneously one is left with a third-order polynomial of the following form:

$$\left(D_{\mathrm{d}}^{\mathrm{n}}\right)^3+\Omega D_{\mathrm{d}}^{\mathrm{n}}-\Psi=0, \tag{41}$$

where

$$\Omega=\frac{6\rho_{\mathrm{g}}^{\mathrm{n}}D_{AB}Sh^*\Delta t}{\rho_{\mathrm{d}}^{\mathrm{n}}}>0, \tag{42}$$

$$\Psi=\frac{\rho_{\mathrm{d}}^{\mathrm{o}}}{\rho_{\mathrm{d}}^{\mathrm{n}}}\left(D_{\mathrm{d}}^{\mathrm{o}}\right)^3>0. \tag{43}$$

The above polynomial is monotonically increasing and therefore, has only one real root given as

$$D_{\mathrm{d}}^{\mathrm{n}}=\left(\frac{\Psi}{2}+X\right)^{1/3}-\left(X-\frac{\Psi}{2}\right)^{1/3}, \tag{44}$$

where X is defined as

$$X=\sqrt{\left(\frac{\Psi}{2}\right)^2+\left(\frac{\Omega}{3}\right)^3}. \tag{45}$$

3.4. Boundary and inlet conditions

A qualitative description of the problem and the boundaries is given in Fig. 2. Fluid exit boundary conditions at the east face are approximated by assuming the flow to be steady state at this location. The north and west face boundaries are treated as free-stream or entrainment boundaries. The momentum and pressure boundaries are defined by assuming constant pressure and the scalar properties are defined by either setting the normal gradient of the property to zero, if the flow is leaving the solution domain, i.e., in positive direction; or defining the parameter as constant and equal to the initial conditions, if the flow is being entrained into the solution domain. These assumptions are likely to introduce errors. The errors have been minimised, by taking the boundaries at a large distance from the flow field of interest, in order to make the conditions as close to the initial conditions as possible.

The south face is the axis of symmetry, which is treated by setting the radial velocity and the gradients of the dependant variables normal to the axis, to zero. In other words, we are assuming no flux normal to the boundary.

Fig. 3 gives the description of the grid. The dilute spray assumption requires a relatively coarse grid structure in the region of the injector, where a dense spray core is usually experienced. In order to satisfy this assumption, a single injection cell is used to introduce the dispersed liquid and continuous gas phases into the solution domain. The grid size and dimensions are described in Table 1. This assumption and approach results in crudely modelled mass and momentum conservation laws in the near-injector flow field. There is no information available for the turbulent flow field close to the injector. The convention adopted by Dunbar and Watkins (1997) is used, where the kinetic energy and its respective rate of dissipation are calculated as follows:

$$k_{\mathrm{inj}}=\frac{3}{2}U_{\mathrm{inj}}^2I_{\mathrm{inj}},\qquad \varepsilon_{\mathrm{inj}}=c_\mu^{0.75}k_{\mathrm{inj}}^{1.5}/\ell_{\mathrm{t}}, \tag{46}$$

where I_{inj} is defined as 0.1, and ℓ_{t} is defined as 10% of the nozzle diameter. Dependence of the results on these arbitrarily chosen values is not validated.

The method adopted by Dunbar and Watkins (1997) is used in the procedure for introduction of droplet parcels. The droplet parcels are randomly introduced at the exit plane of

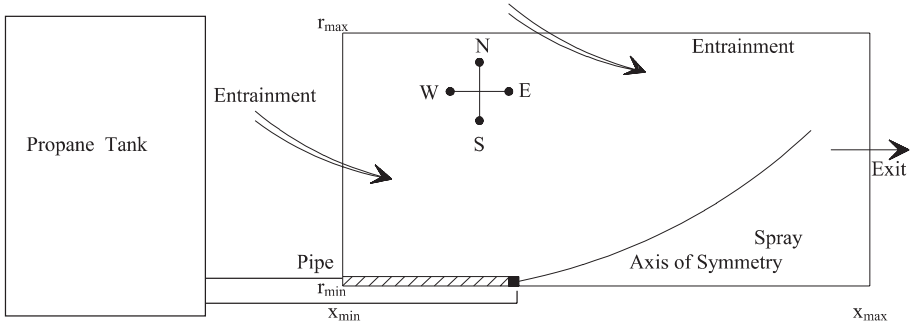

Fig. 2. Problem set-up and boundary conditions.

the injection cell within a region of radius $(r_d)_o$, defined by the spray cone angle, 2β, as follows:

$$(r_d)_o = f_{nd} r_\beta. \tag{47}$$

Here, f_{nd} is a normal distribution random number generator, yielding numbers from zero to one, and r_β is defined as

$$r_\beta = r_{inj} + x_o \tan(\beta), \tag{48}$$

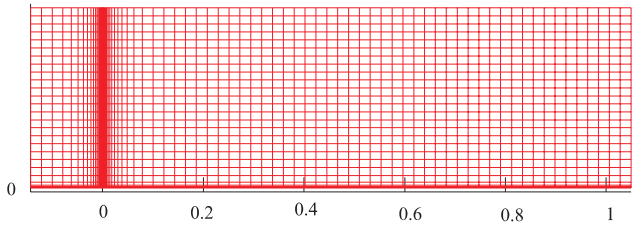

Fig. 3. Final grid structure.

Table 1
Definition of numerical test conditions

Grid parameters	
$i \times j$	120×30
x_{min}	−0.5457 m
r_{min}	0.0 m
x_{max}	2.0 m
r_{max}	0.3 m
Initial parameters	
U_i	0.0 m/s
V_i	0.0 m/s
P_i	1.01×10^5 Pa
T_i	288.0 K
ρ_i	$P_i/(R_{air}\ T_i)$
f_i	0.0
k_i	0.13 m^2/s^2
ε_i	1×10^3 m^2/s^3
Physical parameters	
T_{wb}	231.25 K
n	5
β	15°
Program parameters	
Δt	100.0 μs
t_{max}	2.0 s
$D_{d_{min}}$	0.1 μm

where x_0 is the length of the injection cell. The droplet velocity is calculated from the assumption of conservation of droplet momentum, yielding

$$\begin{aligned} (U_d^n)_k &= U_{inj} \cos\left(\beta \frac{(r_d)_o}{r_{inj}}\right), \\ (V_d^n)_k &= (U_d^n)_k \tan\left(\beta \frac{(r_d)_o}{r_{inj}}\right), \end{aligned} \tag{49}$$

where k represents the class of droplet and U_{inj} is the injection velocity. Detailed numerical test conditions are given in Table 1. A large time step is justified as the maximum value of Courant number reached during the running time is 7.5. All the physical properties of propane are taken as dependent on temperature. In gas phase, vapour–air mixture properties are taken where required.

4. Results and discussion

Propane is initially stored in the pressure vessel, as a saturated liquid, at a pressure corresponding to atmospheric temperature. Figs. 4 and 5 show the quality and the injection velocity from a nozzle of 4 mm diameter, which are required as inlet conditions for the theoretical spray model. Similar results are generated for other nozzle sizes. The quality at the nozzle exit remains constant after the initial discharge of air. Hence the mass transfer rate is independent of the pressure inside the pipe, and so are density and energy. Only the velocity is dependent on the pressure. This gets constant value after 0.25 s, when the system reaches a quasi-steady state. These observa-

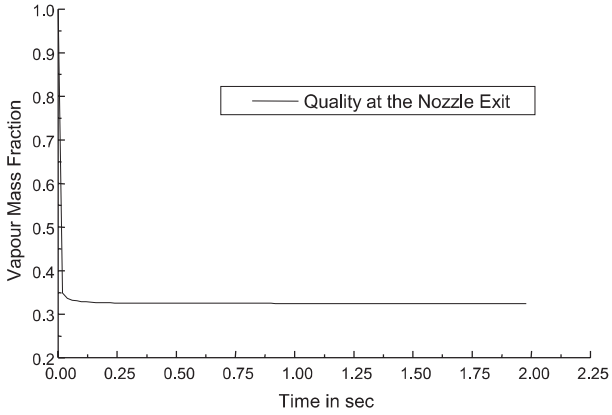

Fig. 4. Profile of the quality of two-phase propane during blowdown at nozzle exit.

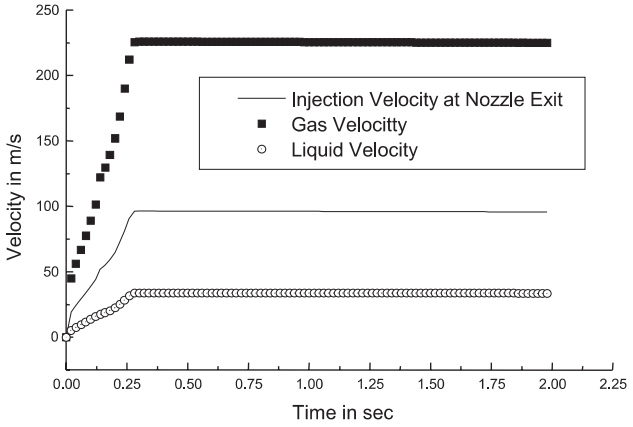

Fig. 5. Profile of the velocity of the two-phase propane during blow-down at nozzle exit.

tions are in line with the findings of Lee et al. (1991), who observed that the pressure in the pressure vessel has large effect on the velocity, rather than on the surfactant concentration.

The gas and liquid velocities are calculated independently, assuming no interactions, i.e., slip conditions. This is unlikely in practice, due to drag effects, therefore we assume a mass-weighted mean velocity for both the gas and the drops. Thus, the injection velocity shown in Fig. 5 is the mass weighted average of the respective velocities.

4.1. Effect of collision and break-up models

Figs. 6–8 show the comparison of the numerical predictions without break-up and collision models and with the original collision model and the modified one. By modified we refer to the model in which time step limitation has been included. Though there is not much difference in the axial velocity profile of the droplets, it is obvious that the modified collision model better predicts the results and the trend in the size distributions, as compared to the predictions made without collision and break-up model. As is obvious from Fig. 6 the basic problem that occurred was in the spread of the spray, which required the authors to insert such modifications.

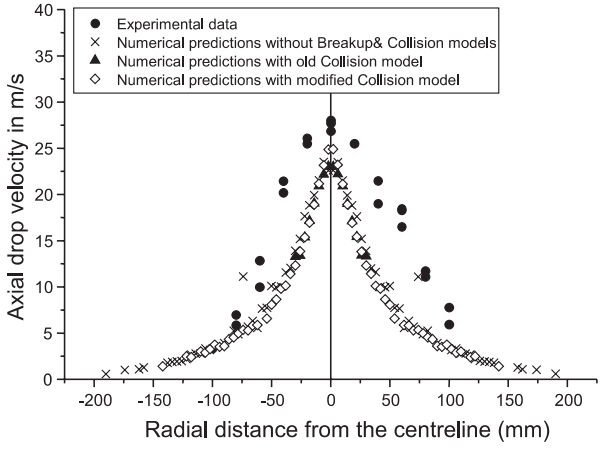

Fig. 6. Axial drop velocity profile at 500 mm from the nozzle.

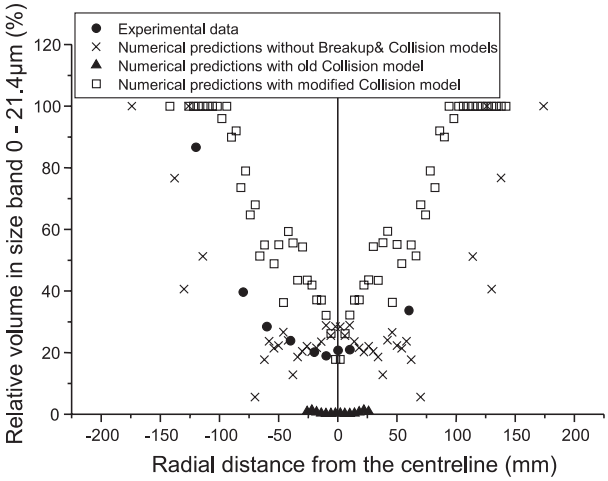

Fig. 7. Lateral droplet size distribution in 0–21.4 μm volumetric diameter band.

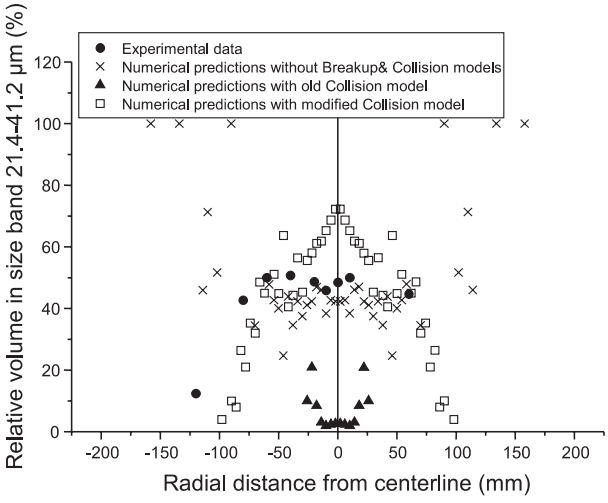

Fig. 8. Lateral droplet size distribution in 21.4–41.2 μm volumetric diameter band.

Drops at 231 K travel within the surrounding temperature of 288 K. With such a high temperature difference, the liquid tends to evaporate at an extremely high rate. Since the drops are assumed to be at their wet bulb temperature corresponding to the atmospheric pressure, there is no increase in the temperature of the liquid. Thus, all the heat transfer from the surroundings is used to evaporate the liquid. Now in such a model the evaporation rate at the periphery will be much higher as compared to the centre where the spray contains higher mass concentration of liquid propane.

Drop coalescence takes place more in the near injector region and in the centre of the spray, where a higher mass concentration of liquid propane is present. The former one was the problem that needed to be addressed, as the enhanced evaporation in the peripheral regions along with the coalescence in the higher liquid concentration regions eliminated the droplet parcels and the number of parcels left were not enough to statistically represent the spray.

O'Rourke and Bracco (1980) model allowed the droplets to coalesce without any time associated with the coalescence, thus over-estimating the coalescence. Their results show an

eight-fold increase in the drop diameter downstream, when injected with a 6 μm drop of diesel in a cold run. In the modified model, a time step limitation associated with the drop coalescence is also taken into account, which states that the computational time step be small compared to the collision time for the droplets. Only after this condition is fulfilled the droplets of the target parcel are allowed to collide with the collector parcel. Again not all the droplets are allowed to collide; the probable number of droplets that coalesce in a time step is calculated, which prevents all the droplets of the target parcel to be removed in the same time step. This means that this model allows the two parcels to move away from each other by the next time step, without wiping out one of them, thus decreasing the coalescence in the near injector region as well as in the centre of the spray.

Fig. 9 shows the comparison between modified and unmodified spray models for a 2 mm diameter nozzle after 0.7 s at 95 mm from the nozzle. It is obvious that the previous collision model tended to enhance the coalescence, and gave two peaks above 60 μm of droplet diameter. The new model greatly reduces the number of large drops, and gives a much more acceptable distribution of drop sizes. Once it was established that the modified collision model works well with propane at given conditions, several runs were made for comparison with the experimental results.

4.2. Comparison with Hervieu-Veneau's (1996) experimental results

Fig. 10 presents the normalised size event comparison at 95 mm from the injector, obtained using the 2 mm diameter nozzle and with 11 bar initial pressure and at $D_{32} = 15$ μm and $D_{32} = 25$ μm. Fig. 11 presents the normalised velocity for the same conditions. The results not only validate the mathematical model used for flow upstream of the nozzle, but also give a qualitative validation for taking the Rosin–Rammler (R–R) droplet size distribution for drop injection at the nozzle exit. The two parameters in Eq. (16), which need to be defined, are n and D_{32}. In the empirical research of the values of these coefficients, no rule is given for their determination (Dunbar and Watkins, 1997). The results drawn up here by the authors have been produced by regulating and adjusting these two R–R parameters. The exponential parameter adjusts the volumetric spread of the droplet size distribution; the higher the value, the less the spread. The best value of n was adjudged to be 5, which was used later in all calculations.

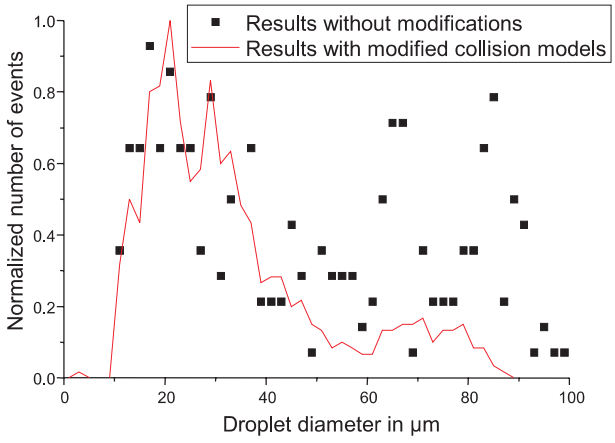

Fig. 9. Comparison between modified and unmodified spray models for 2 mm nozzle after 0.7 s at 95 mm from the nozzle.

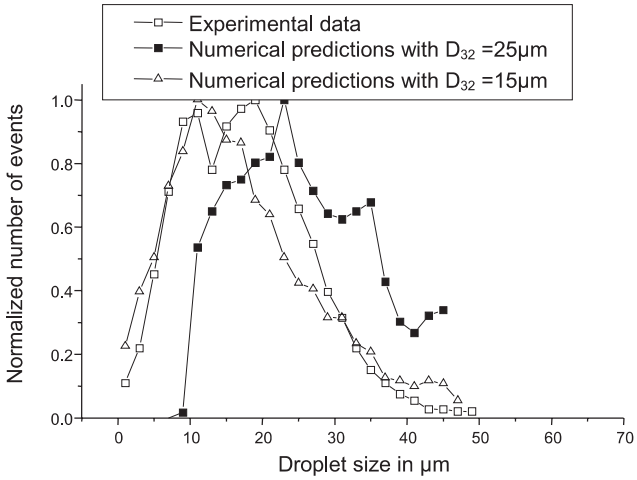

Fig. 10. Normalised droplet size frequency data.

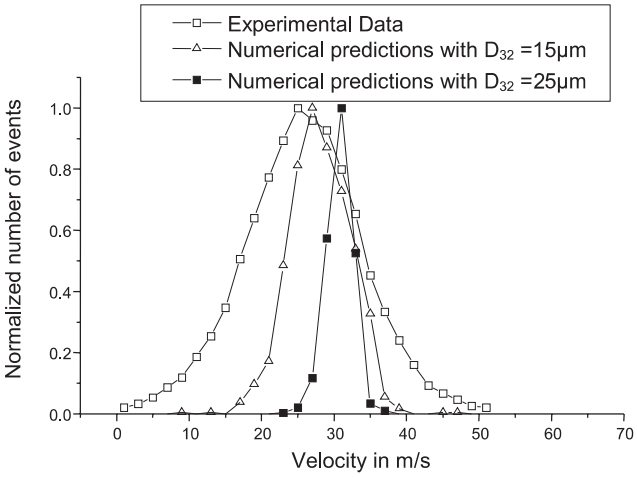

Fig. 11. Normalised axial velocity frequency data.

D_{32} required a lot more consideration. In the absence of an empirical or physical formulation relating the nozzle upstream conditions with droplet sizes produced at nozzle exit for flashing type of atomization, the results of Hervieu-Veneau's (1996) were used to adjust this parameter. From the experimental results it was obvious that the higher is the initial pressure

- more flashing will occur; consequently the fragmentation is more intense and drop sizes will be smaller.
- the larger the diameter of the nozzle, the greater will be the drop sizes.

It is obvious that the numerical results at $D_{32} = 15$ μm are quite accurately predicting the trend. The average arithmetic mean diameter, D_{10}, from numerical considerations using $D_{32} = 15$ μm is 17.4 μm while from experimental data, it is 16.4 μm. Similarly average Sauter mean diameter from experiments is 25.2 μm while the calculated value is 28 μm. The mean axial centreline velocity at 95 mm from the nozzle is 25.36 m/s from experiment, but is 28.07 m/s from the numerical calculations. Though, the overall maximum error involved is 11.1%, yet numerical predictions show lesser spread in the velocity profile.

This may be because the droplet collision and break-up models have no direct influence on the turbulence parameters.

The results obtained from the calculations of the Hervieu-Veneau's (1996) case, led us to take a D_{32} of 25 μm for the larger 4 mm nozzle and storage temperature of 16°C case of HSE described below.

4.3. Comparison with the experimental results from HSE

Fig. 12 shows the axial velocity profiles validated against the experimental data (Allen, 1996a). Axial profiles are plotted at 500 and 1028 mm from the nozzle. The comparison reveals that the theoretical spray model produces similar radial profiles as that obtained experimentally. The predicted centreline axial velocity is under-predicted by 8% at 500 mm; and is over-predicted by 17% at 1028 mm. This shows that experimentally the rate of decrease of the drop velocity is higher than that predicted theoretically. At 95 mm from the nozzle the mean axial centreline velocity is over-predicted; it is under-predicted at 500 mm and then again over-predicted at 1028 mm from the nozzle. It seems that the droplets decelerate slowly to start with, then more rapidly and later slowly again. This would suggest that in the different regions, different effects are dominant. Upstream, where the spray is denser, coalescence and secondary break-up might play a stronger role, whereas further downstream the evaporation could be dominant in the determination of the drops sizes and hence the axial velocity. With the measurements being within the experimental error limits, the predicted results described here represent the experimental data with reasonable accuracy.

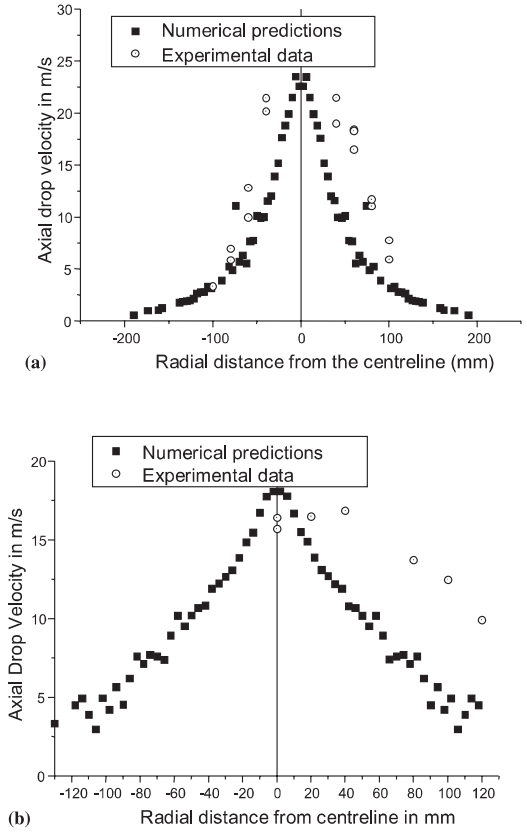

Fig. 12. Axial velocity profiles. (a) 500 mm from the nozzle exit; (b) 1028 mm from the nozzle exit.

Away from the centreline the theory tends to under-predict the experimental results. The disparity can be attributed to the relatively coarse grid in the region not being able to accurately capture the steep property gradients like density. If the grid is fine in the near-injector region, it will tend to fill the cell volumes with the liquid and give negative densities from the pressure equation. This problem is intrinsic in the separated flow model, thus requiring the implementation of a relatively coarse grid in regions of high fluid flow activity. Other contributory factors affect the momentum prediction of the spray model. These are the assumptions of isotropic turbulence in the k–ε model and the turbulence modulation of the gas phase due to the presence of the dispersed liquid phase, which could affect the turbulence micro-scales but would not affect the large eddy structures. These may contribute to the rate of convection and diffusion in the region of axis of symmetry.

The experimental data (Allen, 1996b) gave the relative volume of drops in two size bands of 0–21.4 and 21.4–41.2 μm. The program output was modified to count the number of drops of volumetric mean diameter in the respective band. Relative volume was calculated by dividing with the total volume distribution of the drops sampled in the program. It is therefore, extremely difficult to accurately predict these profiles, as they not only involve the volumetric drop sizes of a parcel in a particular measurement volume, but also the number of droplets in that parcel. With so many variables at ones disposal to be arbitrarily fixed, an accurate set of values, which predicts the profile at all positions, is difficult to get. Yet, in Fig. 13 we manage to predict the trend with reasonable accuracy, apart from the lateral droplet size distribution in 21.4–41.2 μm band at 1088 mm from the nozzle. The experimental profile seems to have changed considerably from 500 to 1088 mm, giving 21% less volume at the centreline for this band while for the smaller band there is an increase of 12% in volume at the centreline. This means that experimentally, the rate of evaporation and hence the rate of decrease in the drop diameter, is much larger as compared to what the evaporation model is predicting here. This could be because the evaporation model described here does not consider any flash evaporation occurring downstream of the nozzle. This cannot be entirely true. Physically, there can be a possibility of the development of regions within the spray, where the vapour concentration around the drop is considerably less resulting into discreet flashing of liquid propane.

There is also some fluctuation in the predictions away from the centreline. A large sample is available near to the axis of symmetry for the statistical analysis. Further from the centre, fluctuations are attributed to the very small sample size available. The remedy to the problem is to introduce a larger number of droplet parcels per time step. But this is limited by the computer power available. A larger number of droplet parcels introduced per time step means a lot more calculations. Already these results with 15 droplet parcels introduced per time step has taken more than 60 CPU hours on a Sun Enterprise 450 machine. An attempt was made to increase the droplet parcels introduced to 30 but the CPU time required increased by 10 fold.

The droplet size distribution profiles have been obtained by taking the Sauter mean diameter of 25 μm and volume distribution parameter of $n = 5$, at the inlet, in the Rosin–Rammler distribution. Hence the profiles shown are dependent on these two factors. A relatively independent solution would require a theoretical model or correlation presenting the Sauter mean diameter at the nozzle exit.

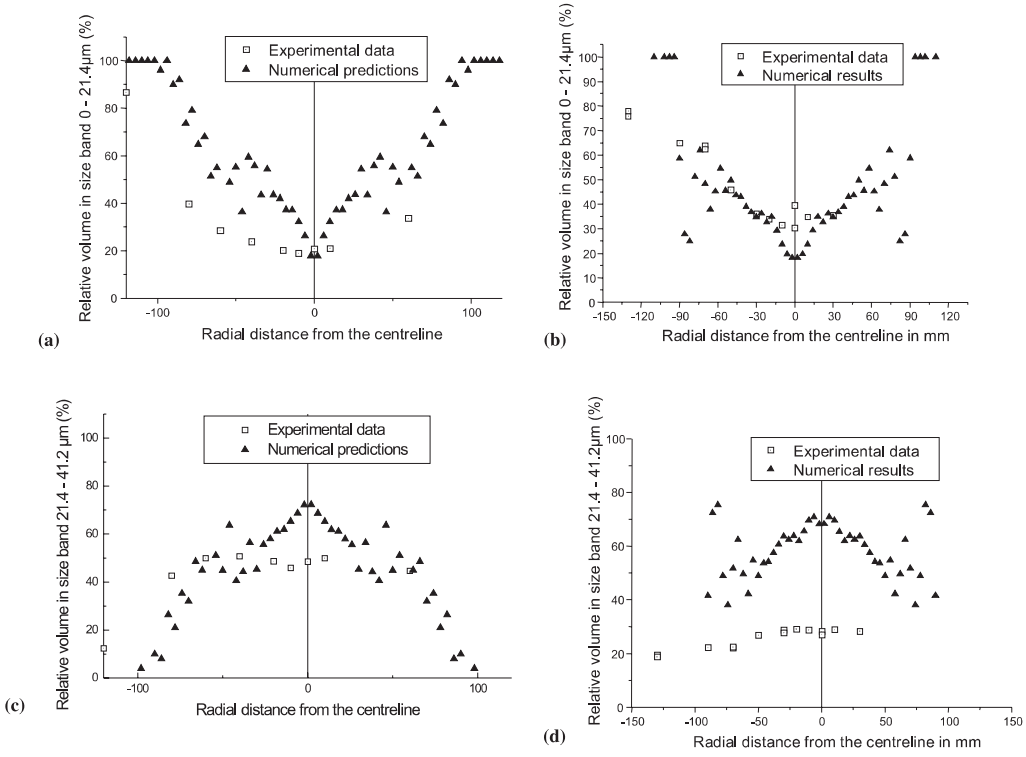

Fig. 13. Lateral droplet size distribution in 0–21.4 and 21.4–41.2 μm volumetric diameter. (a) and (c) 500 mm from the nozzle; (b) and (d) 1088 mm from the nozzle.

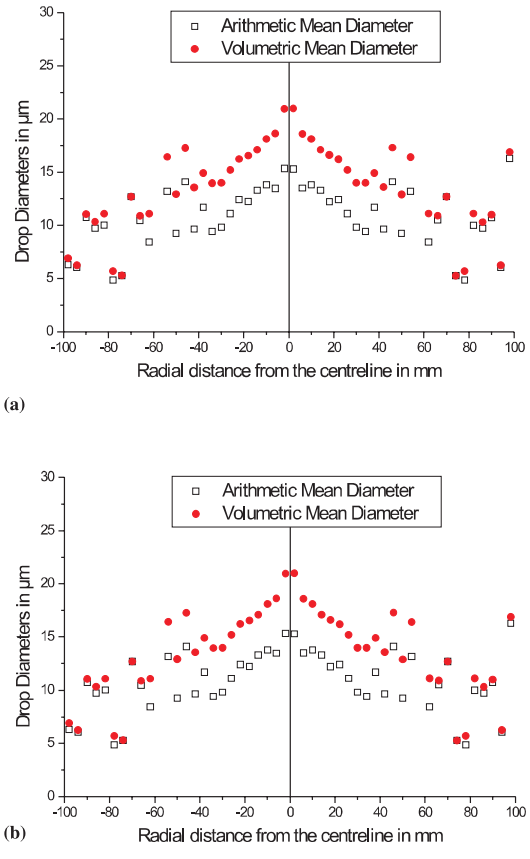

Fig. 14. Theoretical profiles of D_{10} and D_{30}. (a) 500 mm from the nozzle; (b) 1088 mm from the nozzle.

If we consider these numerical results as being sufficiently accurate, then Fig. 14 shows the theoretical profile of the lateral droplet size distribution at 500 and 1088 mm from the nozzle. These give a clearer picture of the spray being modelled.

5. Conclusion

1. Because of the unavailability of any experimental flow field data near the nozzle, the results of the thermodynamic model used could not be verified. Nearest results available for the velocity distribution of drops were those at 95 mm from the nozzle. The results at this distance from the nozzle were used to qualitatively validate the thermodynamic model.
2. The theoretical spray model captured the droplet velocity and size in space with a reasonable degree of success.
3. The implementation of the two theoretical models used to describe the fluid flow from the pressure vessel to the nozzle and the resultant spray transport did not produce an autonomous code. It required the input of empirical parameters in the Rosin–Rammler distribution of drop sizes at the inlet and the spray cone angle as well as the turbulence parameters of turbulence intensity and turbulence length scale.
4. The predicted spatial distribution at the downstream, peripheral locations were not statistically representative, due to the difficulty in accruing large numbers of ensembled droplet parcels in the region over a finite CPU time.
5. Experimental data of Allen (1996a,b) gave only the distributions of relative volumes in the two size bands of 0–21.4 and 21.4–41.2 μm, the profiles of which are difficult to predict.

The future work includes usage of a nonisotropic turbulence model, investigation into a relatively more autonomous code and a better statistical representation of drop sizes at peripheral locations.

References

Aamir, M.A., Watkins, A.P., 1998. CFD Analysis of spray evolution on depressurisation of highly pressurised liquid propane. In: Proceedings of the 14th ILASS Europe Conference, Manchester.

Allen, J.T., 1996a. Laser-Based velocity measurements in two-phase flashing propane jet releases. Health and Safety Laboratory, IR/L/FR/96/5.

Allen, J.T., 1996b. Laser-Based droplet size measurements in two-phase, flashing propane jet releases. Health and Safety Laboratory, IR/L/FR/96/6.

Bettis, R.J., Jaggers, S.F., 1992. Some experimental aspects of transient releases of pressurised liquefied gases. I Chem E. Symp. Series 130, 211–227.

Chen, J.R., Richardson, S.M., Saville, G., 1995. Modelling of two phase blowdown from pipelines-I. A hyperbolic model based on variational principles. Chem. Engrg. Sci. 50 (4), 695–713.

Dunbar, C.A., Watkins, A.P., 1997. Theoretical investigation of the spray from a pressurised metered-dose inhaler. Atomization and Sprays 7 (4), 417–436.

Faeth, G.M., 1983. Evaporation and combustion of sprays. Prog. Energy Combust. Sci. 9, 1–76.

Fauske, K.H., 1965. Two-phase and two- and one component critical flow. Symposium on Two Phase Flow G101–114.

Gosman, A.D., Ioannides, E., 1981. Aspects of computer simulation of liquid fuelled combustors. AIAA Paper No. 81-0323.

Graziadio, M., Andreussi, P., Tognotti, L., Zanelli, S., 1987. Atomisation of coal-water fuels by a pneumatic internal mixing nozzle. Part I-Two-phase flow inside the nozzle. Atomisation and Spray Technol. 3, 187–208.

He, L., Ruiz, F., 1995. Effect of cavitation on flow and turbulence in plain orifices for high-speed atomisation. Atomisation and Sprays 5, 569–584.

Hervieu, E., 1991. Behaviour of a flashing liquid within a vessel following loss of containment. Application to Propane, Final Report, CEC Program: Major Technological Hazards, Contract No. AA-EV4T 00 19-F/GR-764279.

Hervieu, E., 1992. Behaviour of a flashing liquid within a vessel following loss of containment: application to propane. In: ANS Proceedings, 1992 National Heat transfer Conference, 227–235.

Hervieu, E., Veneau, T., 1996. Experimental determination of the droplet size and velocity distributions at the exit of the bottom discharge pipe of a liquefied propane storage tank during a sudden blowdown. J. Loss Prev. Process Ind. 9 (6), 413–425.

Issa, R.I., 1986. Solution of implicitly discretised fluid flow equations by operator-splitting. J. Comp. Phys. 62 (1), 40–65.

Khaleghi, H., 1990. Three-dimensional modelling and comparison with experiments of sprays and gas flow in test rigs and diesel engines. Ph. D. Thesis, UMIST, Manchester.

Launder, B.E., Spalding, D.B., 1972. Lectures in Mathematical Models of Turbulence. Academic Press, London.

Lee, K.C., Suen, K.O., Yianneskis, M., 1991. Characterisation of evaporating sprays from metered dose-inhalers by LDA. In: Proceedings of the fourth International Conference on Laser Anemometry, Adv. and Appl., Ohio.

Lees, F.P., 1980. Loss Prevention in the Process Industries. Butterworth Publishers, Oxford.

Nicholls, H., 1972. Stream and droplet break-up by shock waves, NASA SP-194.

O'Rourke, P.J., Bracco, F.V., 1980. Modelling of drop interactions in thick sprays and comparison with experiment. Stratified Charge Automotive Engines Conf., IMechE, Paper No. C404/80.

Orme, M., 1997. Experiments on droplet collisions, bounce, coalescence and disruption. Prog. Energy Combust. Sci. 23, 65–79.

Pereira, J.C.F., Chen, X.-Q., 1996. Numerical calculations of unsteady heavy gas dispersion. J. Hazardous Mater. 46, 253–272.

Reitz, R.D., Diwakar, R., 1986. Effect of droplet break-up on fuel sprays. SAE paper No. 860469.

Schmidt, D.P., Rutland, C.J., Corradini, M.L., 1999. A fully compressible, two-dimensional model of small, high-speed, cavitating nozzles. Atomisation and Sprays 9, 255–276.

Vandroux-Koenig, S., Berthoud, G., 1997. Modelling of a two phase momentum jet close to the breach, in the containment vessel of a liquefied gas. J. Loss Prev. Process Ind. 10 (1), 17–29.

Wang, D.M., 1992. Modelling spray wall impaction and combustion processes of diesel engines. Ph.D. Thesis, UMIST, Manchester.